

GALACTIC WIND SIGNATURES AROUND HIGH REDSHIFT GALAXIES

DAISUKE KAWATA^{1,2} AND MICHAEL RAUCH¹,
Draft version November 28, 2021

ABSTRACT

We carry out cosmological chemodynamical simulations with different strengths of supernova (SN) feedback and study how galactic winds from star-forming galaxies affect the features of hydrogen (HI) and metal (CIV and OVI) absorption systems in the intergalactic medium at high redshift. We find that the outflows tend to escape to low density regions, and hardly affect the dense filaments visible in HI absorption. As a result, the strength of HI absorption near galaxies is not reduced by galactic winds, but even slightly increases. We also find that a lack of HI absorption for lines of sight (LOS) close to galaxies, as found by Adelberger et al., can be created by hot gas around the galaxies induced by accretion shock heating. In contrast to HI, metal absorption systems are sensitive to the presence of winds. The models without feedback can produce the strong CIV and OVI absorption lines in LOS within 50 kpc from galaxies, while strong SN feedback is capable of creating strong CIV and OVI lines out to about twice that distance. We also analyze the mean transmissivity of HI, CIV, and OVI within $1 h^{-1}$ Mpc from star-forming galaxies. The probability distribution of the transmissivity of HI is independent of the strength of SN feedback, but strong feedback produces LOS with lower transmissivity of metal lines. Additionally, strong feedback can produce strong OVI lines even in cases where HI absorption is weak. We conclude that OVI is probably the best tracer for galactic winds at high redshift.

Subject headings: galaxies: kinematics and dynamics — galaxies: formation — galaxies: stellar content

1. INTRODUCTION

Supernova (SN) explosions are thought to be capable of ejecting part of the interstellar medium (ISM) from galaxies. Such outflows are often called “galactic winds” (Johnson & Axford 1971; Mathews & Baker 1971; Veilleux et al. 2005). Galactic winds are believed to be an important mechanism for enriching the intergalactic medium (IGM) (Ikeuchi 1977; Aguirre et al. 2001; Madau et al. 2001; Scannapieco et al. 2002; Cen et al. 2005) and are thought to play a crucial role in shaping the mass-metallicity relation of galaxies (e.g. Larson 1974; Dekel & Silk 1986; Arimoto & Yoshii 1987; Gibson 1997; Kawata & Gibson 2003), and in heating the IGM (Ikeuchi & Ostriker 1986). Galactic winds have been observed in local star-forming galaxies (e.g. Lynds & Sandage 1963; Martin 1998; Ohya et al. 2002), where their outflow morphology and kinematics have been extensively studied (e.g. Martin 2005; Rupke et al. 2005). Some local galaxies show outflows to about 20 kpc (Veilleux et al. 2003). Such outflows are expected to be more common at high redshift, where star formation is more active ($z > 1$) (Madau et al. 1996). Galactic winds are also believed to terminate star formation in ellipticals (Mathews & Baker 1971; Kawata & Gibson 2003) and have been invoked at high redshift to explain the high age of their stellar populations (Kodama & Arimoto 1997; Labbé et al. 2005; Kriek et al. 2006). Theoretical studies suggest that for progenitors of disk galaxies the gas outflow due to SN heating at high redshift can effectively suppress star formation, leading to a less dense stellar halo (Brook et al. 2004) and a larger disk (Sommer-Larsen et al.

2003; Robertson et al. 2004; Governato et al. 2006) at $z = 0$. Therefore, observing galactic wind signatures at high redshift may elucidate an important ingredient in the formation of galaxies.

The observational studies at high redshift have uncovered evidence that outflows from star-forming galaxies at high redshift may be common, as has been shown for Lyman break selected galaxies (e.g. Pettini et al. 1998; Ohya et al. 2003; Shapley et al. 2003). These results have contributed to the debate about how the outflows from star-forming galaxies may affect the intergalactic medium (IGM). Rauch et al. (2001a) uncovered evidence for repeated injection of kinetic energy into higher density, CIV absorbing gas, possibly driven by recent galactic winds. In a study of the *lower density*, general Lyman alpha forest, Rauch et al. (2001b) found that most of the HI absorption systems lack signs for being disturbed by winds, and derived upper limits on the filling factor of wind bubbles. Simcoe et al. (2002) surveyed the properties of strong OVI absorption systems at high redshift and proposed that the apparent temperatures and the kinematics of the OVI gas as well as their rate of incidence could be explained if massive Lyman break galaxies are driving winds out to 50 proper kpc.

Adelberger et al. (2003, 2005a) studied the absorption line features in the spectra of background QSOs whose line of sight (LOS) passes close to Lyman-break selected star-forming galaxies. They found a deficit of neutral hydrogen near these galaxies out to $0.5 h^{-1}$ comoving Mpc, accompanied by a surplus of HI beyond that radius, and suggested that most Lyman break galaxies may reside bubbles where superwinds have depleted the HI in the interior and piled up more neutral gas beyond the hot bubble. The more recent, more statistically significant of these studies Adelberger et al. (2005a) however, does not support this claim, but still appears to show a sig-

¹ The Observatories of the Carnegie Institution of Washington, 813 Santa Barbara Street, Pasadena, CA 91101

² Swinburne University of Technology, Hawthorn VIC 3122, Australia

nificant fraction (about 7 out of 24) of the LOS exhibiting weak or no absorption within $1 h^{-1}$ comoving Mpc. Numerical simulations of the IGM without SN feedback predict a much lower fraction of such weak absorption systems near the galaxies (Kollmeier et al. 2003), a fact that may conceivably be explained if at least some galaxies have outflows destroying HI in the IGM in their vicinity. Adelberger et al. (2003, 2005a) also show that there is a correlation between the spatial distribution of CIV absorption lines and the star-forming galaxies, with the strongest CIV absorption lines being observed at the LOS closest to the galaxies (~ 80 proper kpc). This result may indicate that outflows related to recent star formation activity have enriched the IGM locally. Other evidence for the association of CIV with galaxies has been reported (Pieri et al. 2006; Simcoe et al. 2006). Scannapieco et al. (2006b) compared the observed LOS correlation functions of CIV and SiIV with analytic outflow models and concluded that the observed correlation can be formally explained if there are outflows with a scale of about 2 comoving Mpc from large galaxies whose stellar mass is about $10^{12} M_{\odot}$. However, the large range of the individual wind bubbles required to explain the CIV-galaxy correlation is puzzling. Theoretical arguments suggest that the clustering of CIV with Lyman break galaxies is not necessarily proof that those same galaxies produced the metal enrichment (Porciani & Madau 2005; Scannapieco 2005), and the relation between metals in the IGM and galaxies clearly needs further study.

Cosmological numerical simulations have proven a useful tool for understanding metal absorption lines (Rauch et al. 1997). Comparisons between the observations and the statistics of metal absorption lines derived from numerical simulations have mostly been concerned with measurements of the metallicity and ionization state of the IGM (e.g. Davé et al. 1998; Aguirre et al. 2002; Schaye et al. 2003; Aguirre et al. 2004). The relation between star-forming galaxies and absorption line features have recently been studied by a number of authors (Croft et al. 2002; Kollmeier et al. 2003; Bruscoli et al. 2003; Kollmeier et al. 2006; Tasker & Bryan 2006), with several papers (e.g. Croft et al. 2002; Kollmeier et al. 2006; Theuns et al. 2002) considering observable effects of galactic outflows on the Lyman alpha forest absorption lines. These studies generally have concluded that such outflows hardly affect the strength of the HI absorption lines, because the winds tend to escape into less dense regions and do not impact the IGM where the density is high enough to produce HI absorption lines.

So far, most studies based on full-blown cosmological numerical simulations have focused on HI absorption lines. Although there have been a number of papers discussing the origin and properties of metal absorption lines (e.g. Rauch et al. 1997; Theuns et al. 2002; Aguirre et al. 2005; Tasker & Bryan 2006; Oppenheimer & Davé 2006), the relation between metal absorption line systems and outflows from the coeval galaxy population has remained largely unclear, in particular as the effect of winds on the physical properties of metal lines it is not well known. Nevertheless, the fact that the metallicity is expected to be increased by galactic outflows, and the availability of multiple transitions and several heavy elements with a different enrichment history should make metal lines a potentially much more

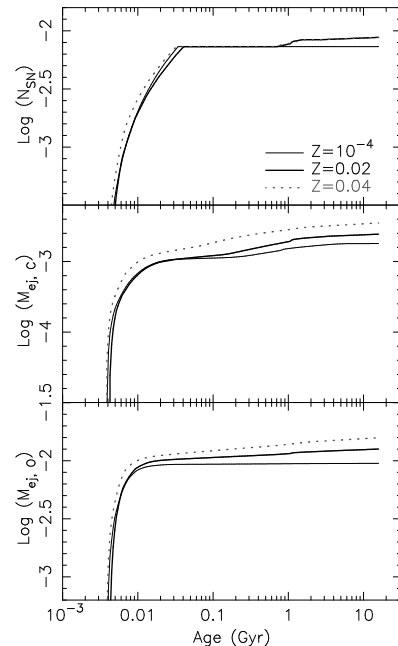


FIG. 1.— Number of SN and chemical yields as a function of the age of a star particle with a mass of $1 M_{\odot}$. The upper panel shows the total number of SN. The middle and lower panels present the total ejected carbon and oxygen masses, respectively. The thin solid, thick solid, and gray thick dotted lines indicate the history of a star particle with the metallicity of $Z = 10^{-4}$, 0.02, and 0.04, respectively.

useful tracer of galactic winds than neutral hydrogen.

The current paper studies the properties of both HI and metal absorption lines, and looks for observational signatures of galactic winds. To this end, we run cosmological simulations with the original version of the Galactic Chemodynamics Code, GCD+ (Kawata & Gibson 2003) which is capable of tracing the chemical evolution of the IGM and galaxies self-consistently. We carry out simulations with different strengths of SN feedback, and compare the features of the HI and metal absorption lines between the simulations, attempting to identify features sensitive to the presence of galactic winds.

The following section will explain our method including the description of the numerical simulations with GCD+ and analysis of absorption lines. Unlike previous studies, we follow different heavy elements separately, and take into account the abundance evolution for the different elements when creating fake QSO spectra from the simulation. This is important because the different elements come from different types of SNe or are due to mass loss from inter-mediate mass stars with different life-times. Section 3 shows our results. First, Section 3.1 focuses on one galaxy in the simulation volume, and compares the absorption line features around the galaxy among models with different SN feedback strengths. Then, in Section 3.2 we discuss the results more quantitatively using artificial QSO spectra in 1000 random LOS. Section 4 summarizes our conclusions.

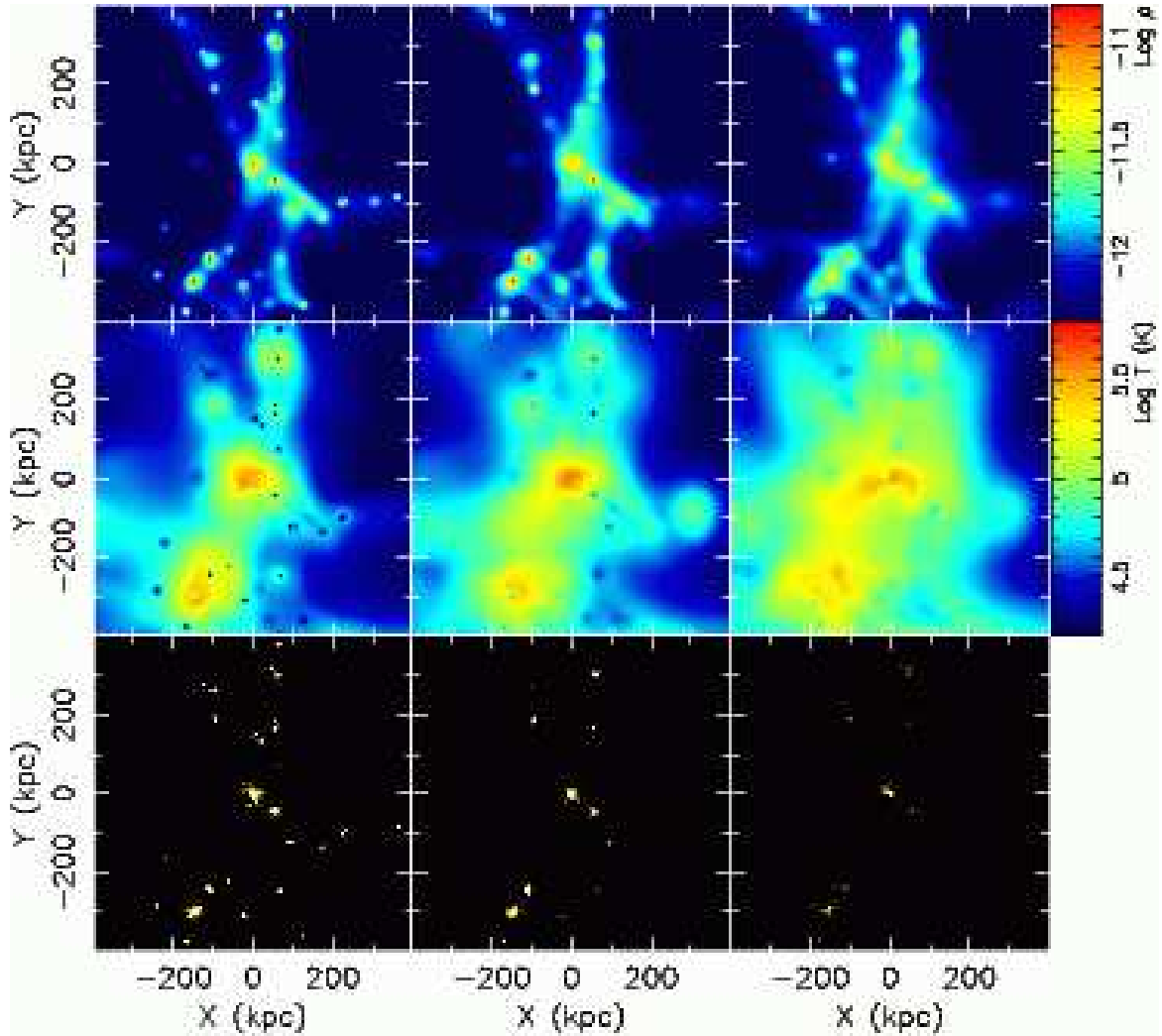


FIG. 2.— Projected gas surface density (upper) and temperature (middle) map and star particle distribution (lower) for models NF (left), SF (middle), and ESF (right).

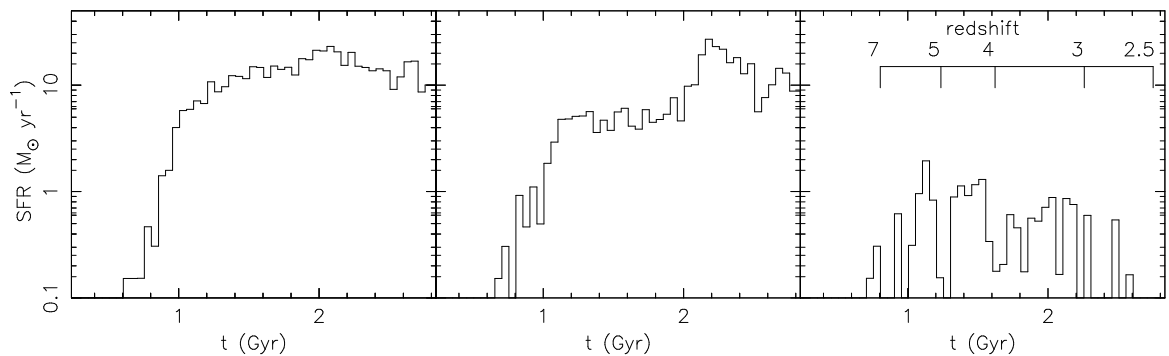


FIG. 3.— The history of the star formation rate down to $z = 2.43$ for models NF (left), SF (middle), and ESF (right). The time of first star formation is different among the three models, although there should not be any difference before feedback from stars happens. This difference is because different models are carried out on different computers, and the star formation model in GCD+ uses the random number generator (see Kawata & Gibson 2003, for details) whose sequences are different for different simulations.

2. METHOD

2.1. Numerical Simulations

The simulations were carried out using the Galactic Chemodynamics Code GCD+ (Kawata & Gibson 2003). GCD+ is a three-dimensional tree N -body/smoothed particle hydrodynamics (SPH) code that incorporates self-gravity, hydrodynamics, radiative cooling, star forma-

tion, SN feedback, and metal enrichment. GCD+ takes into account chemical enrichment by both Type II (SNe II) (Woosley & Weaver 1995) and Type Ia (SNe Ia) (Iwamoto et al. 1999; Kobayashi et al. 2000) SNe and mass loss from intermediate-mass stars (van den Hoek & Groenewegen 1997), and follows the chemical enrichment history of both the stellar and gas components of the system. Figure 1 shows the total number of SN

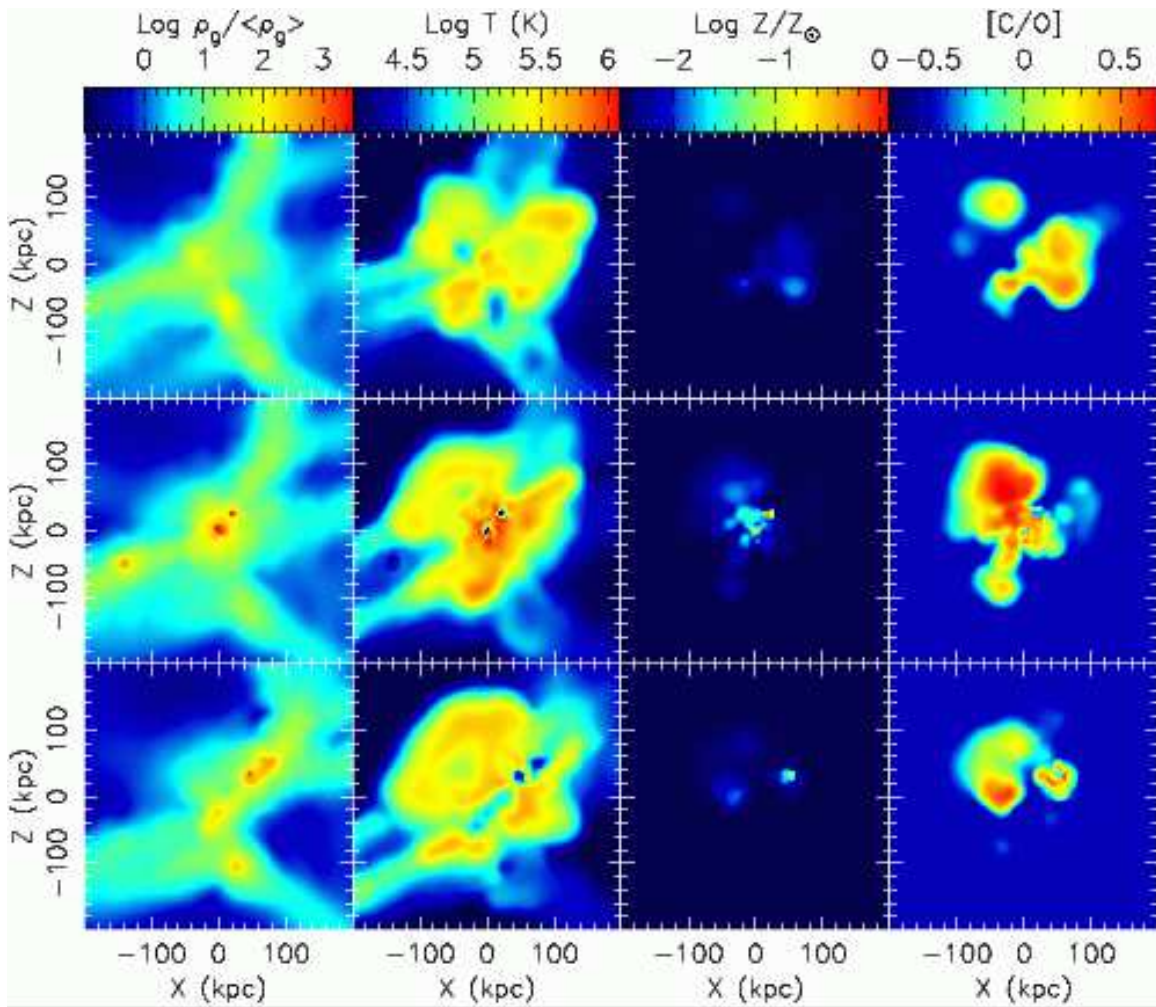


FIG. 4.— Overdensity, temperature, metallicity, and [C/O] map (from left to right) for model NF at $Y = +50$ (upper), 0 (middle) -50 (lower) proper kpc, where the biggest galaxy is set to be at the center.

TABLE 1
PROPERTIES OF THE CENTRAL GALAXY AT $z = 2.43$

Model Name	E_{SN} (erg)	$M_{\text{vir}}^{\text{a}}$ (M_{\odot})	$r_{\text{vir}}^{\text{b}}$ (kpc)	$M_{\text{gas, vir}}$ (M_{\odot})	$M_{\text{DM, vir}}$ (M_{\odot})	$M_{\text{star, vir}}$ (M_{\odot})	M_{200}^{c} (M_{\odot})	$T_{\text{vir}}^{\text{d}}$ (K)
NF	0	2.1×10^{11}	57	1.7×10^{10}	1.7×10^{11}	2.5×10^{10}	2.0×10^{11}	3.8×10^5
SF	3×10^{51}	2.0×10^{11}	57	1.5×10^{10}	1.7×10^{11}	1.6×10^{10}	1.9×10^{11}	3.7×10^5
ESF	5×10^{51}	1.7×10^{11}	56	1.2×10^{10}	1.6×10^{11}	1.7×10^9	1.6×10^{11}	3.2×10^5

^aVirial Mass in the definition of Kitayama & Suto (1996)

^bVirial radius in the definition of Kitayama & Suto (1996)

^cMass within a radius which is the radius of a sphere containing a mean density of 200 times the critical density at $z = 2.43$

^dVirial temperature in the definition of Kitayama & Suto (1996)

(both SN II and SN Ia) and the total amount of carbon and oxygen ejected from a star particle with the mass of 1 M_{sun} as a function of its age. Initially, SNe II go off, and they continue until the 8 M_{sun} star dies (~ 0.04 Gyr in the case of $Z = 0.02$). There is no SN until SNe Ia start to occur around 0.7 Gyr. A star particle with $Z = 10^{-4}$ does not lead to SN Ia, because the adopted SNIa model restricts the metallicity range for progenitors of SN Ia to $\log Z/Z_{\odot} > -1.1$ (see Kobayashi et al. 2000, for details). Oxygen is produced mainly

by SN II. After SN II ceases, the continuous ejection of oxygen and carbon is mainly due to the contribution from intermediate-mass stars. Although oxygen yield is mainly from the pre-enriched ejecta, carbon is newly processed in intermediate-mass stars, which explains the significant yield in the low metallicity case.

The adopted version of the code also includes non-equilibrium chemical reactions of hydrogen and helium species (H , H^+ , He , He^+ , He^{++} , H_2 , H_2^+ , H^-) and their cooling processes, following the method of Abel et al.

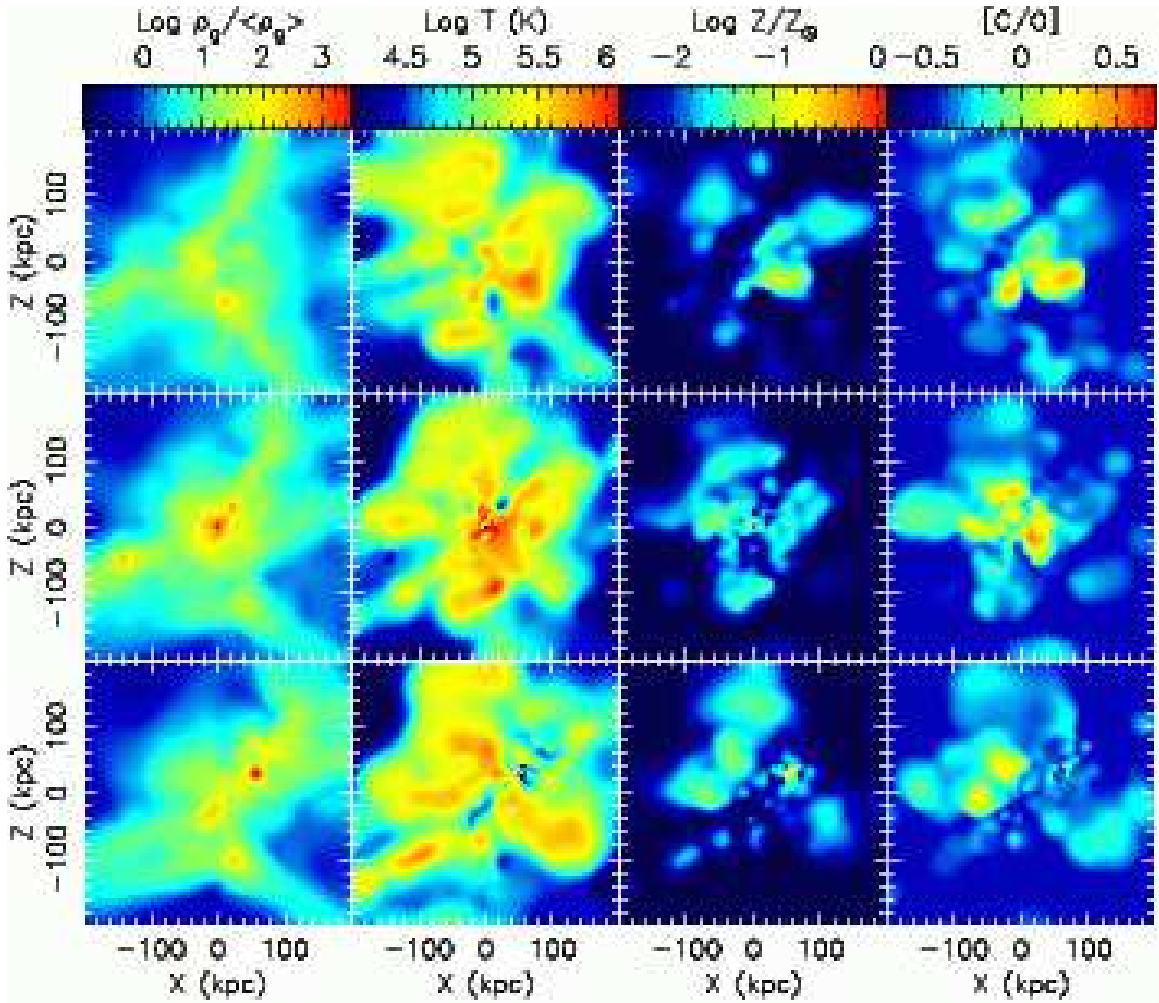


FIG. 5.— Same as Fig. 4, but for model SF.

(1997); Anninos et al. (1997); Galli & Palla (1998). The details of the non-equilibrium chemical reactions are described in the Appendix of Kawata et al. (2006). We have made the following update from the code used in Kawata et al. (2006). We adopt a density threshold for star formation, and permit star formation from gas whose hydrogen number density ($n_{\text{H}} = f_{\text{H}}\rho_{\text{g}}/m_{\text{p}}$, where f_{H} , ρ_{g} and m_{p} are the hydrogen mass fraction, density, and proton mass for each gas particle) is higher than 0.01 cm^{-3} (Schaye 2004). It is also crucial to take into account the effect of the UV background radiation when studying the properties of the IGM. We use the UV background spectrum suggested by Haardt & Madau (2001). The code follows non-equilibrium chemical reactions of hydrogen and helium species subjected to the UV background. In addition, radiative cooling and heating due to heavy elements are taken into account based on the Raymond-Smith code (Raymond & Smith 1977), used in Cen et al. (1995). The simulation starts at $z = 29.7$, and initial temperature and the fractions of hydrogen and helium species are calculated by RECFAST (Seager et al. 1999, 2000). We turn on the UV background radiation at $z = 6$ (Becker et al. 2001; Fan et al. 2001).

The cosmological simulation adopts a Λ -dominated cold dark matter (Λ CDM) cosmology ($\Omega_0=0.24$, $\Lambda_0=0.76$, $\Omega_{\text{b}}=0.042$, $h = 0.73$, $\sigma_8 = 0.74$, and $n_s = 0.95$)

consistent with the measured parameters from three-year *Wilkinson Microwave Anisotropy Probe* data (Spergel et al. 2006). We use a multi-resolution technique to achieve high-resolution in the regions of interest, including the tidal forces from neighboring large-scale structures. The initial conditions for the simulations are constructed using the public software LINGER and GRAFIC2 (Bertschinger 2001). Gas dynamics and star formation are included only within the relevant high-resolution region ($\sim 6 \text{ Mpc}$ at $z=0$); the surrounding low-resolution region ($\sim 55 \text{ Mpc}$) contributes to the high-resolution region only through gravity. Consequently, the initial condition consists of a total of 1350380 dark matter particles and 255232 gas particles. The mass and softening lengths of individual gas (dark matter) particles in the high-resolution region are 7.61×10^6 (3.59×10^7) M_{\odot} and 1.15 (1.93) kpc, respectively. The high-resolution region is chosen as the region within 8 times the virial radius of a small group scale halo with the total mass of $M_{\text{tot}} = 3 \times 10^{12} M_{\odot}$ and the virial radius of $r_{\text{vir}} = 380 \text{ kpc}$ at $z = 0$.

We simulate the following three models with these initial conditions to investigate the effect of SN feedback. Model NF is a "no-SN-feedback" model: although the model follows the chemical evolution due to SNe and mass loss from stars, we ignore the effect of energy feed-

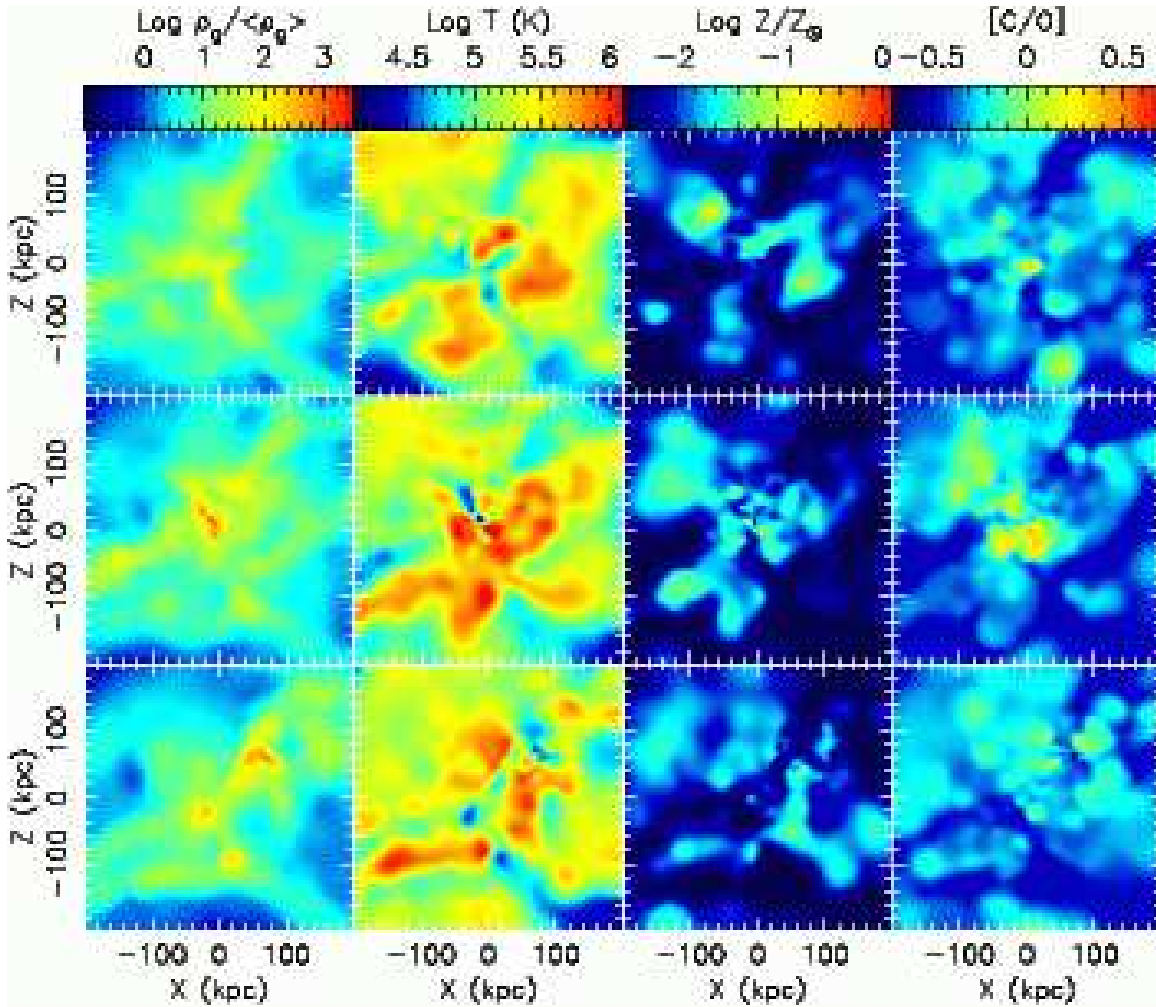


FIG. 6.— Same as Fig. 4, but for model ESF.

back by SNe. Model SF is a “strong feedback” model, where each SN yields the thermal energy of 3×10^{51} erg. This model produces a feedback effect noticeable in a number of observables. In the final model, ESF, for “extremely strong feedback” model, a thermal energy release of 5×10^{51} erg per SN is assumed. We found that this model causes too strong effects of feedback, and produces too few stars. Therefore, the model is obviously unrealistic. However, we retain the model for this extreme case to help put the other models in perspective.

We analyze the properties of the IGM for all the models at $z = 2.43$. As mentioned above, we adopt the multi-resolution technique. We extract a spherical volume within the radius of $r_p = 800$ kpc (in physical scale at $z = 2.43$) from a galaxy in the high-resolution region. The central galaxy is the biggest galaxy in the simulation volume, and the radius is chosen to avoid contamination from the low-resolution particles. In this paper, we use the coordinate system where the central galaxy resides at $(x,y,z)=(0,0,0)$. Figure 2 shows the gas density, temperature, and stellar density map of the central 800×800 proper kpc^2 region of this volume analyzed for all the models. Figure demonstrates that the stronger feedback affects the gas density distribution, and suppresses star formation more dramatically.

2.2. The Artificial QSO Spectra

The aim of this paper is to search for signatures of galactic winds among the absorption lines in the background QSO spectrum. To this end, we construct artificial QSO spectra, with lines of sight through the simulation volume from various orientation and projected positions, and compare the absorption line features among models with different strengths of SN feedback. For a given line of sight we identify the gas particles whose projected distance is smaller than their SPH smoothing length. In this paper, we focus on three absorption features, HI_{1216} , CIV_{1548} , and OVI_{1032} , and we call them HI, CIV, and OVI hereafter. The ionization fractions for HI, CIV, and OVI for each gas particle are derived as follows. The HI fraction is self-consistently calculated in our simulations, because GCD+ follows the non-equilibrium chemical reactions of the hydrogen and helium ions. The CIV and OVI fractions for each gas particle are analyzed with version 6.02b of CLOUDY, described by Ferland et al. (1998), assuming the condition of optical thin and ionization equilibrium. Here, we put in the density, temperature, and the abundances of different elements for the gas particles in the simulation, and run CLOUDY adopting the same UV background radiation as used in the simulations (Haardt & Madau 2001). Unfortunately, we realized that even our (unrealistically) strong feed-

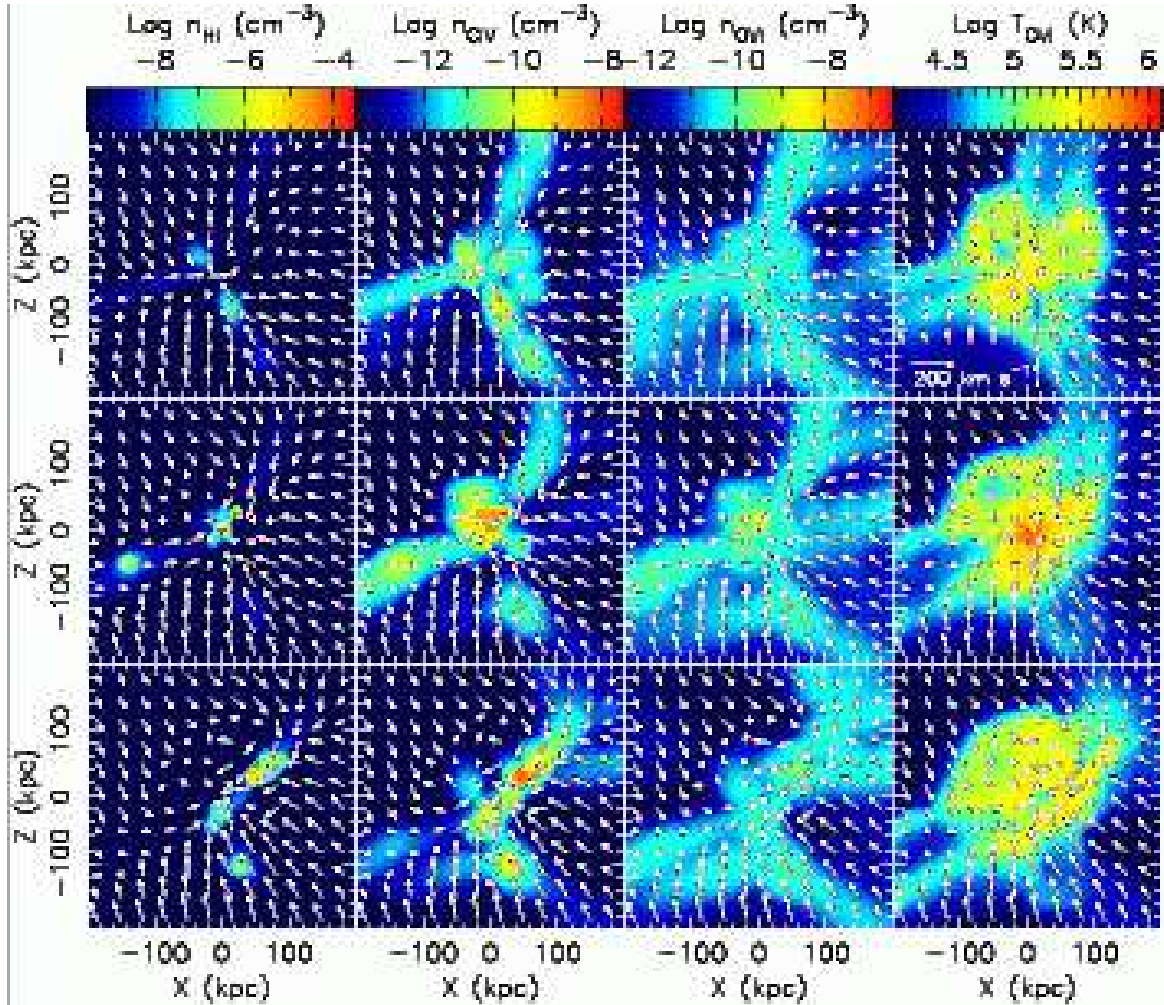


FIG. 7.— Density of HI, CIV, and OVI and OVI weighted temperature map (from left to right) for model NF at $Y=+50$ (upper), 0 (middle) -50 (lower) proper kpc, where the biggest galaxy is set to be at the center. The arrows represent the velocity field weighted by HI, CIV, OVI, and OVI in the panels from left to right, respectively. The size of arrow corresponds to the amount of velocity, as indicated in the upper right panel.

back model cannot enrich the lower density regions in the IGM as much as what is observed (Cowie & Songaila 1998; Schaye et al. 2003; Aguirre et al. 2004). For example, some filaments are not enriched at all even in models ESF as will be seen in Figure 6, although quantitative comparisons with the observational data (see also Oppenheimer & Davé 2006) will be pursued in a future paper. This is likely because the limited resolution of our simulations is unable to resolve the formation of smaller galaxies which form at a higher redshift and could enrich the IGM. Thus, to mimic pre-enrichment for the low density regions we add metals at the level of $[C/H]=-3$ and $[O/H]=-2.5$ to all gas particles. Once the ionization fractions are obtained, the column densities at the LOS for each species are analyzed for each gas particle, using the two-dimensional version of the SPH kernel. The optical depth $\tau(\nu)$ profiles along the LOS are calculated by the sum of the Voigt-absorption profiles for each particle, taking into account their temperature and LOS velocity, $v_{i,LOS}$, which is the sum of Hubble expansion and peculiar velocity. The final spectra are constructed, assuming an overall signal-to-noise ratio of 50 per 0.04 \AA pixel, the read out signal-to-noise ratio 500, and FWHM=6.7 km s^{-1} . We stress that we take into account the difference between carbon and oxygen abundances in our

chemodynamical simulations, when obtaining CIV and OVI fraction.

Note that the simulation volume analyzed is only 1.6 proper Mpc scale at $z = 2.43$. The Hubble expansion at $z = 2.43$ is $236 \text{ km s}^{-1} \text{ Mpc}^{-1}$ in the adopted cosmology, and 1.6 proper Mpc corresponds to 378 km s^{-1} . In addition, since the volume is overdensity region, the expansion velocity is smaller than the Hubble expansion. In Section 3.2, we analyze the mean transmissivity within $1 h^{-1}$ comoving Mpc from the galaxies. The velocity that corresponds to $1 h^{-1}$ comoving Mpc is 94.2 km s^{-1} at $z = 2.43$, which is well within the range of the volume. However, in the real Universe, if there are absorbers outside the volume at the LOS and their peculiar velocity is large, they can contribute to absorptions in the velocity range we focus on (see Kollmeier et al. 2003, for more detailed discussion of such effect). Therefore, we ignore the contamination from such absorptions, and consider the ideal absorption systems only by the absorbers which are spatially close.

3. RESULTS

3.1. Absorption features around a galaxy

To study how the gas outflows from galaxies affect the absorption line features, we generate two sets of QSO

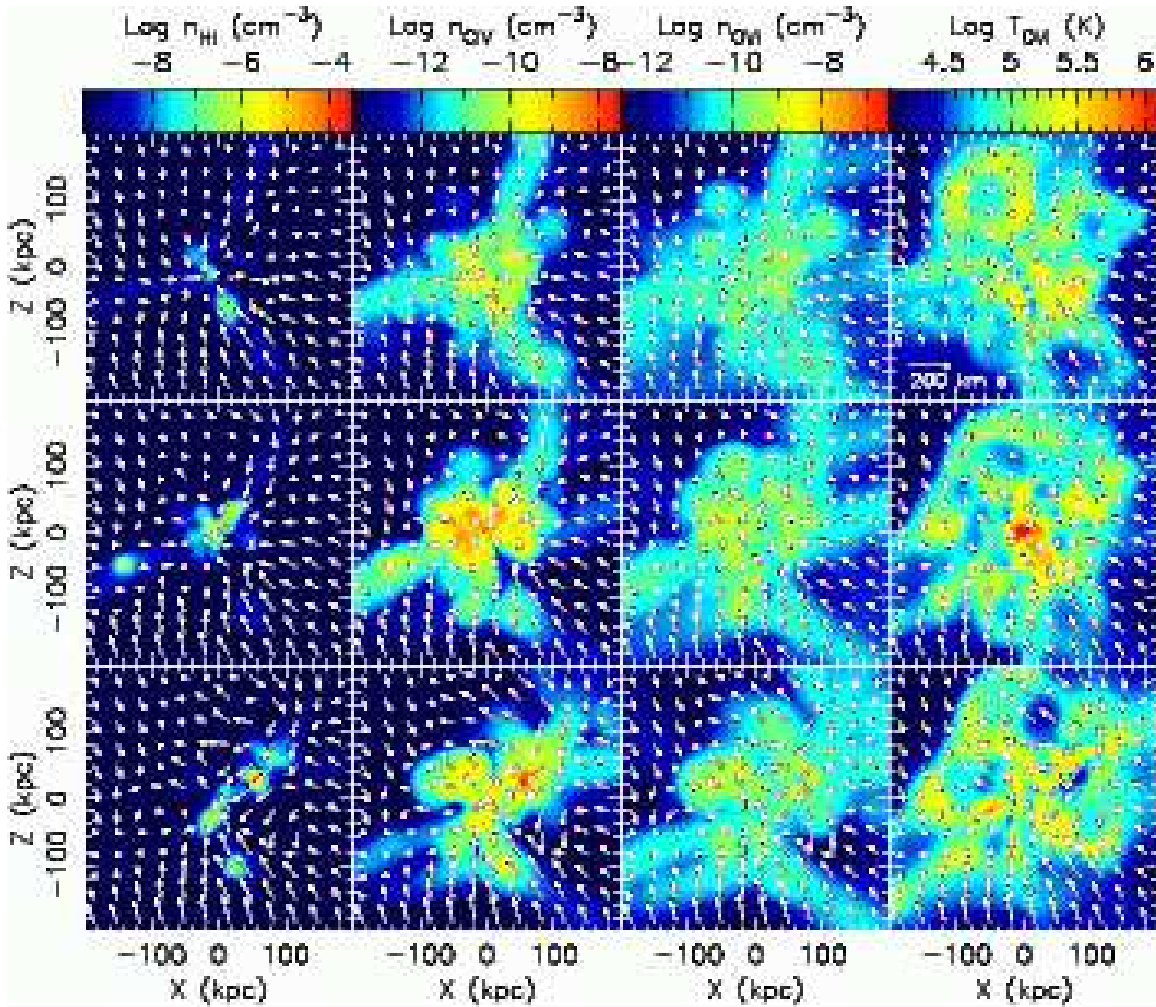


FIG. 8.— Same as Fig. 7, but for model SF.

spectra for all the models. In this section, we analyze the spectra whose LOS are chosen as the 5×5 grid points each separated by 50 kpc (in physical scale at $z = 2.43$) as projected onto the plane of the sky. The grid is centered on a galaxy. In the next section, we generate 1000 random LOS spectra, and compare them among the three models. The properties of the central galaxy chosen for the present section for different feedback models are summarized in Table 1. The total mass of the central galaxy is slightly smaller than the estimated mass of the BX galaxies ($M_{200} \sim 6.3 \times 10^{11} - 1.6 \times 10^{12} M_{\odot}$ in Adelberger et al. 2005b) from the observational studies of the IGM-galaxies connection around $z = 1.9 - 2.6$ (Adelberger et al. 2003, 2005a; Simcoe et al. 2006). However, the accurate mass range for such rest-frame UV-selected galaxies are still unknown. In this paper, we simply assume that the central galaxy is a typical UV-selected star-forming galaxies, and our simulation volume is a typical environment for such galaxies. This assumption will be tested in our future studies. Figure 3 shows the history of the total star formation rate for the star particles within $r = 5$ proper kpc at $z = 2.43$. The extremely strong feedback in model ESF terminates star formation in the system. We confirmed that SNe Ia continuously heat the ISM, which keeps maintaining an outflow in model ESF.

We chose the X–Y plane in Figure 2 as the projected plane of the sky, and define the Z-axis as the LOS direction. Figures 4–6 demonstrate the overdensity, temperature, metallicity, and abundance ratio of carbon to oxygen, [C/O], in the X–Z plane at three different position of $Y = \pm 50$ and 0 proper kpc for models NF, SF, and ESF, respectively. In the same planes, Figures 7–9 give the density distributions of HI, CIV, and OVI, and the OVI weighted temperature map. In these figures, the velocity field of the gas component is also shown with tangential arrows.

In model NF the central galaxy ends up surrounded by a hot gaseous halo with a radius of about 100 kpc (Fig. 4). This is due to infalling gas being shock-heated to the virial temperature (Table 1). This situation appears common for high redshift galaxies (Rauch et al. 1997) and corresponds to the hot accretion mode of (Kereš et al. 2005; Dekel & Birnboim 2006)

Because of the inflow, the metallicity of the hot gas is low. On the other hand, the high density filaments are cold, and part of the gas keeps accreting through the filaments onto the galaxy, i.e., the cold accretion mode described by Kereš et al. (2005) and Dekel & Birnboim (2006) (see also the velocity field in Fig. 7). As a result, the HI density is higher along the filament, and gets significantly higher in the collapsed region near the central

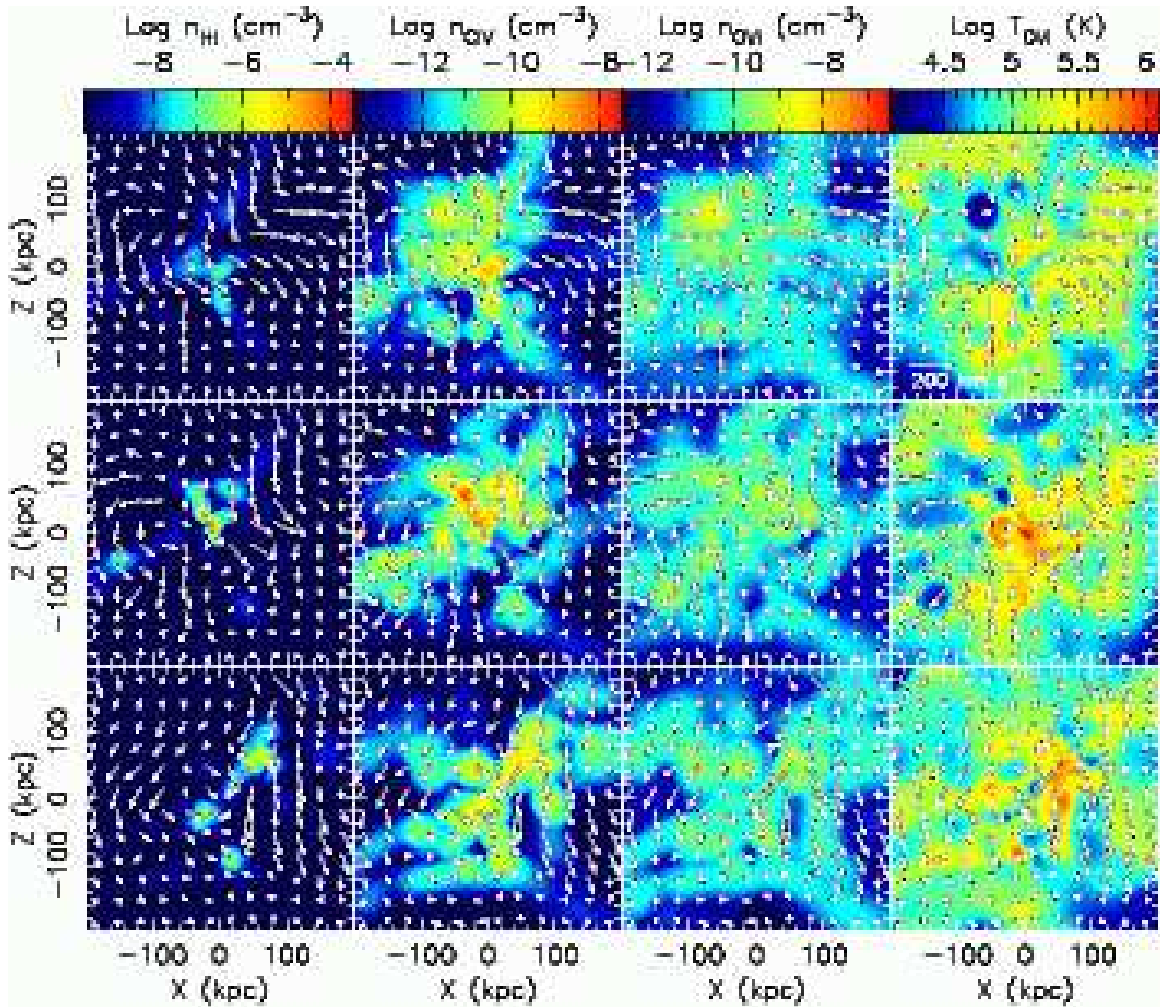


FIG. 9.— Same as Fig. 7, but for model ESF.

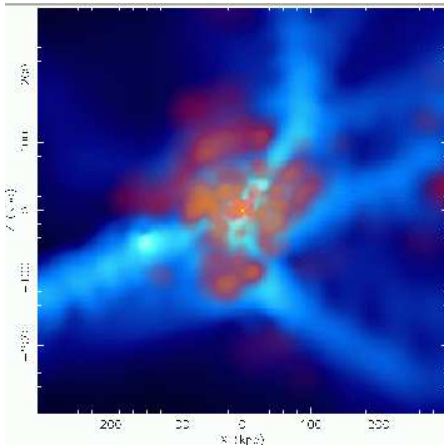


FIG. 10.— Composite image of overdensity (blue contour) and metallicity (red contour) distribution at $Y=0$ for model SF. The edges of contours for overdensity and metallicity correspond to $\log \rho_g / \langle \rho_g \rangle = -1$ and $\log Z/Z_\odot = -2.5$, respectively.

galaxy and the neighboring galaxies. The spatial distribution of CIV and OVI also traces the filaments, and their densities are high in the region close to the galaxies.

Model SF produces a more extended hot gas region than model NF, and the hot gas is now metal-enriched (Fig. 5), compared to the NF case. Here the hot gas is dominated by a galactic wind induced by strong SN feed-

back. The temperature map of Figure 5, the arrows in Figure 8, and Figure 10 demonstrate that the enriched gas tends to escape toward the lower density regions. The filament remains unaffected by the wind. As a result, the cold accretion is still maintained through the filaments, which continues funneling gas to the galaxy. This is similar to what was observed in previous numerical simulations with strong feedback effect (e.g., Theuns et al. 2002; Kollmeier et al. 2006). Consequently, the distribution of HI density is not significantly different from model NF. On the other hand, higher density CIV and OVI gas extends over a much larger region. This is because the enriched gas is blown out from the galaxy, and helps to raise the abundance of carbon and oxygen in the IGM.

Interestingly, we find that the gas whose OVI density is high in model SF has a low temperature which is consistent with photoionization equilibrium for OVI (typical logarithmic temperatures are around $\text{Log}(T(\text{K})) = 4.2$) as opposed to collisional ionization temperature (typical $\text{Log}(T(\text{K})) = 5.5$). Comparison between the 3rd and 4th columns in Figure 8 demonstrates that the region where the density of OVI is high has temperatures around $\text{Log}(T(\text{K})) < 4.5$. This is gas that has been blown out of the galaxy, and cooled down by radiative cooling after colliding with the ambient IGM. CIV in low density halo

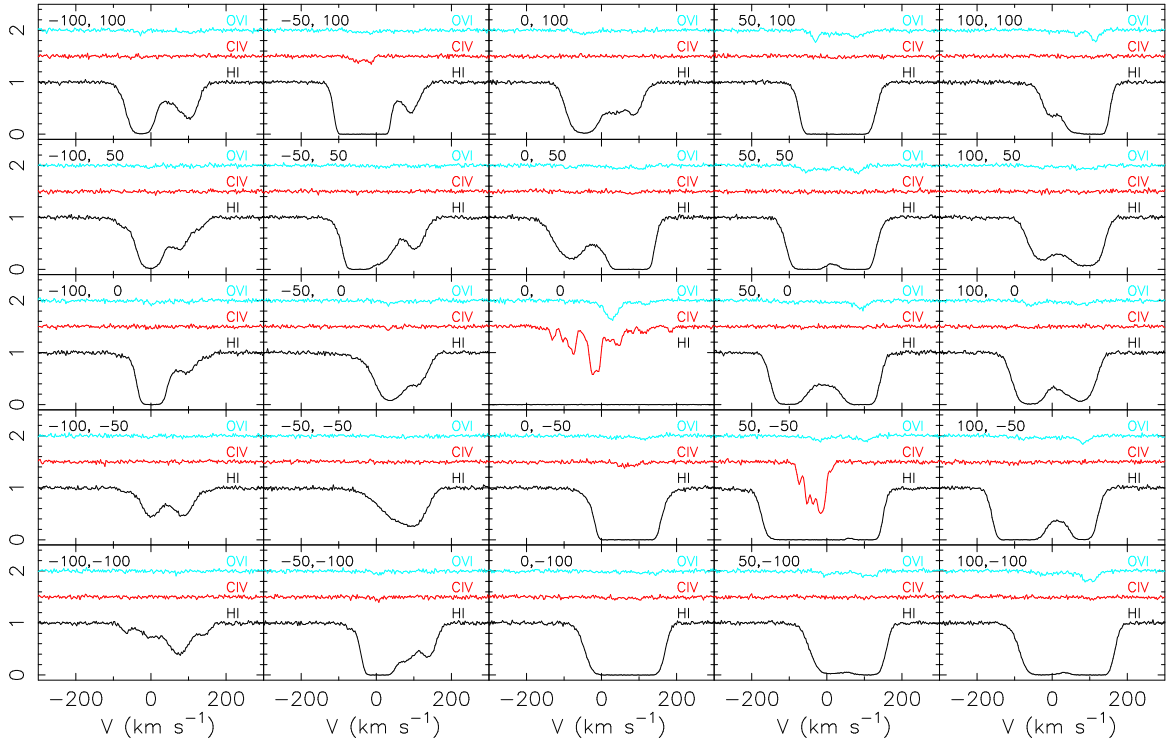


FIG. 11.— Mosaic of 5×5 lines of sight spectra of HI, CIV, and OVI lines around a galaxy at $z = 2.43$ for model NF. The central panel corresponds to the position of the galaxy, and each line of sight is separated by 50 kpc in physical scale. The numbers at the upper left corner of each panel present the (x,y) coordinate (in kpc) for each LOS. In the case of CIV and OVI only the stronger line of each doublet is shown. The LOS velocity is adjusted so that the LOS velocity of the galaxy equals zero.

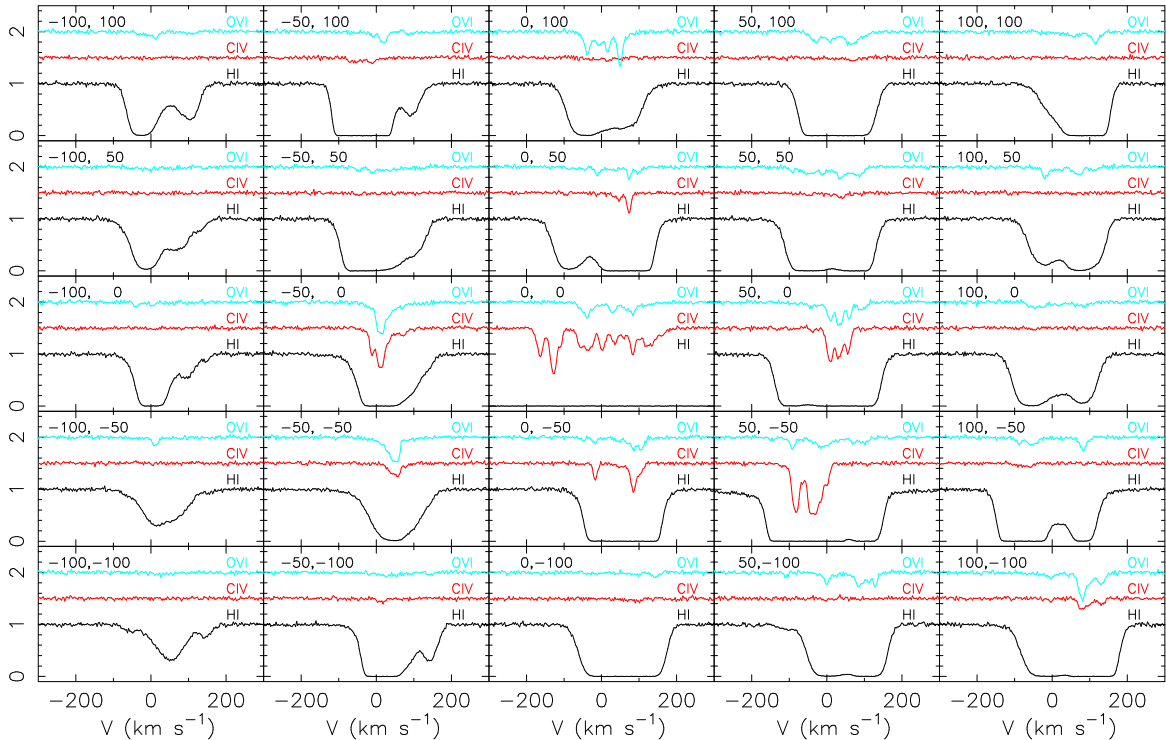


FIG. 12.— Same as Fig. 11, but for model SF.

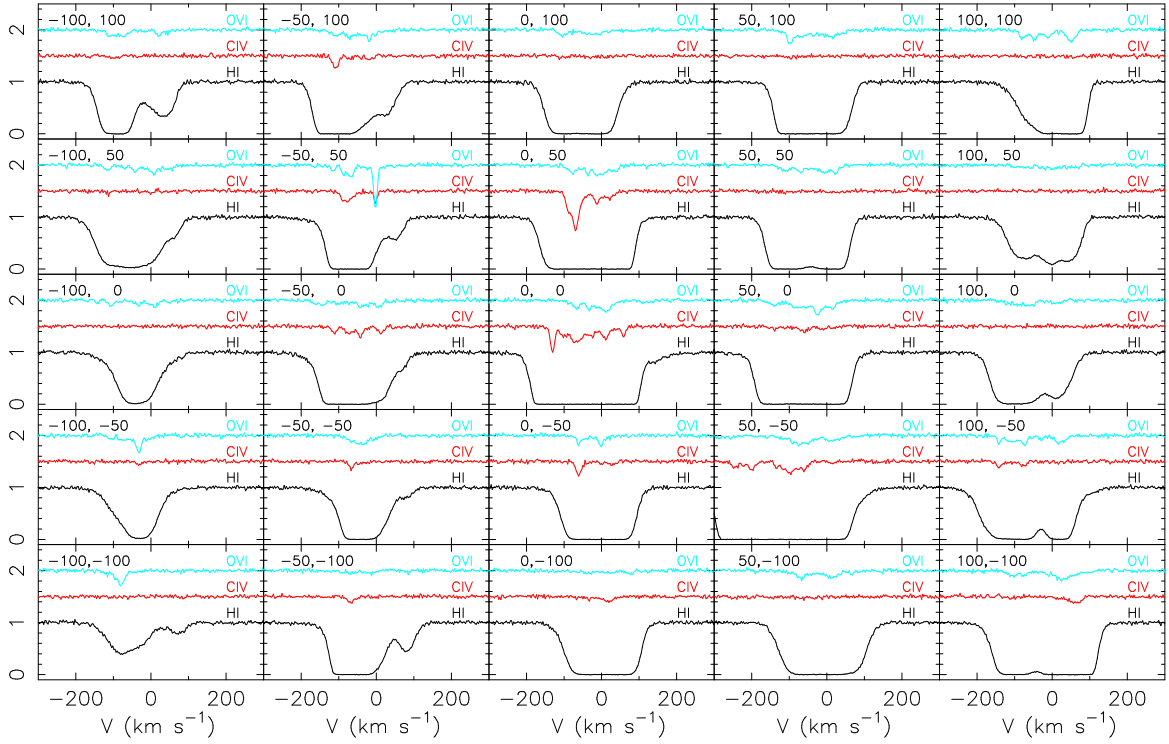


FIG. 13.— Same as Fig. 11, but for model ESF.

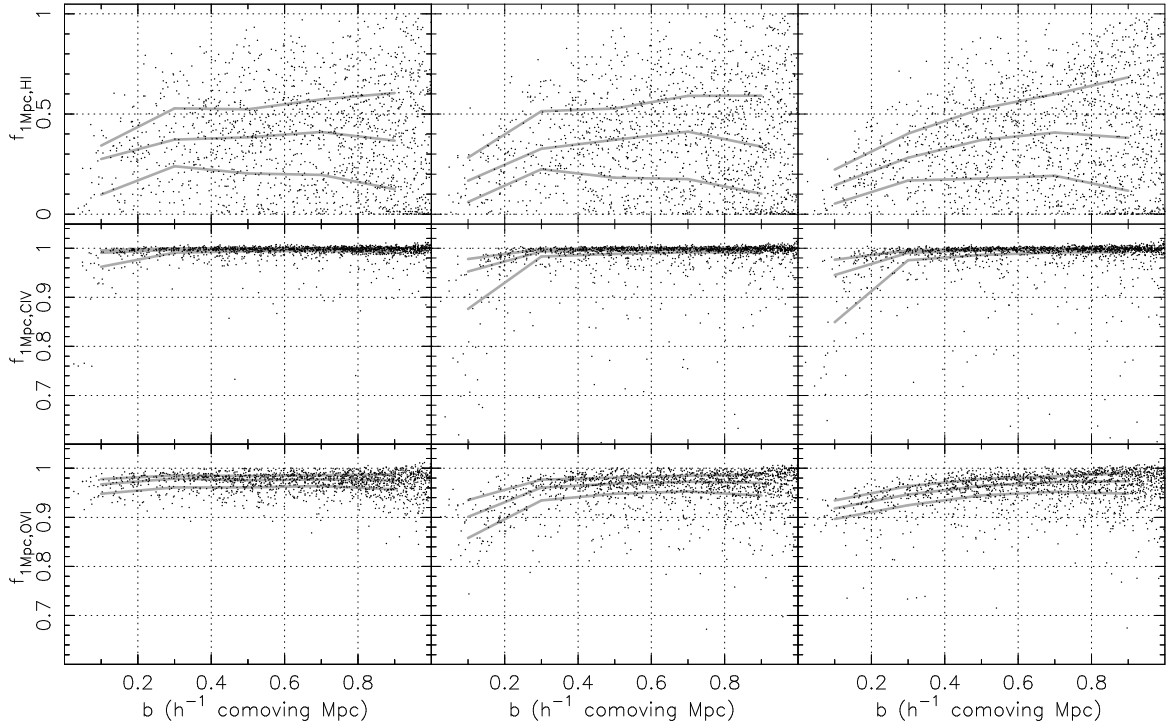


FIG. 14.— The mean transmissivity of HI (upper), CIV (middle), and OVI (lower) for the pixels within $1 h^{-1}$ comoving Mpc of the galaxies as a function of the impact parameter for models NF (left), SF (middle), and ESF (right). The gray lines indicate median and 25th and 75th percentile. Note that the scale of the y-axis, i.e., $f_{1\text{Mpc}}$ is different in each panel.

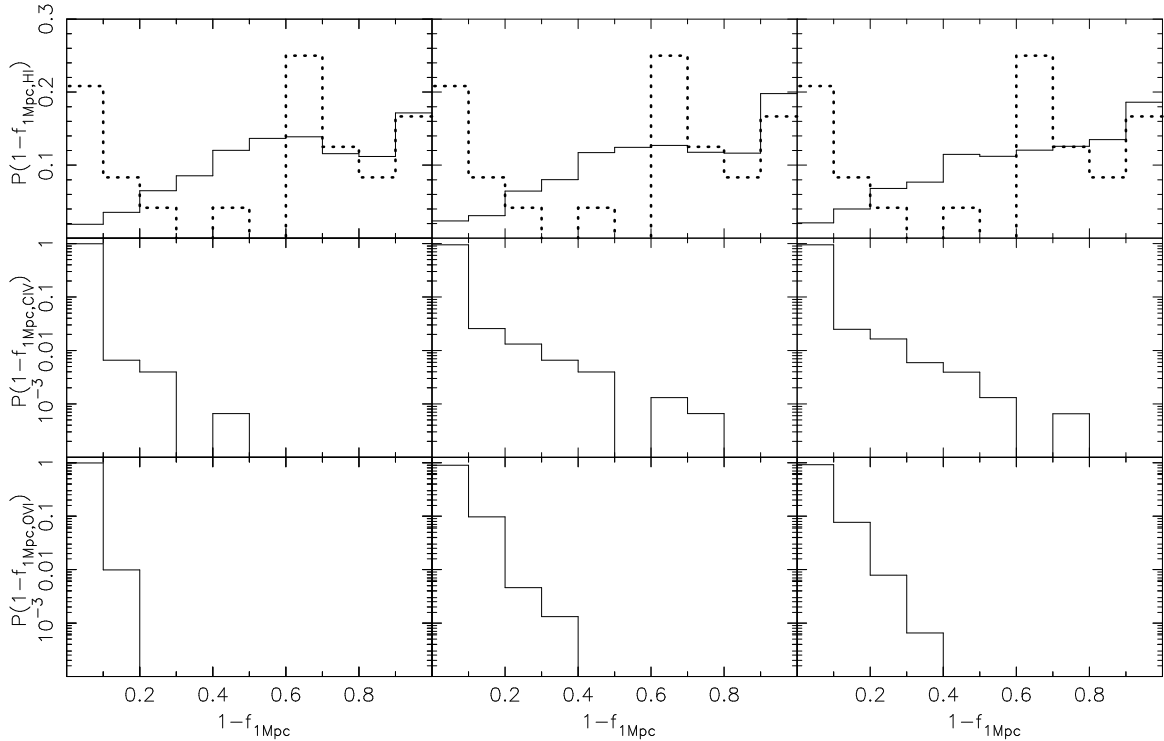


FIG. 15.— The probability of the flux decrement $1 - f_{1\text{Mpc}}$ of HI (upper), CIV (middle), and OVI (lower), where $f_{1\text{Mpc}}$ is the mean transmissivity for the pixels within $1 h^{-1}$ comoving Mpc of the galaxies. The left/middle/right panel shows the results of model NF/SF/ESF. The dotted histogram in the upper panels present the observational results of Adelberger et al. (2005a).

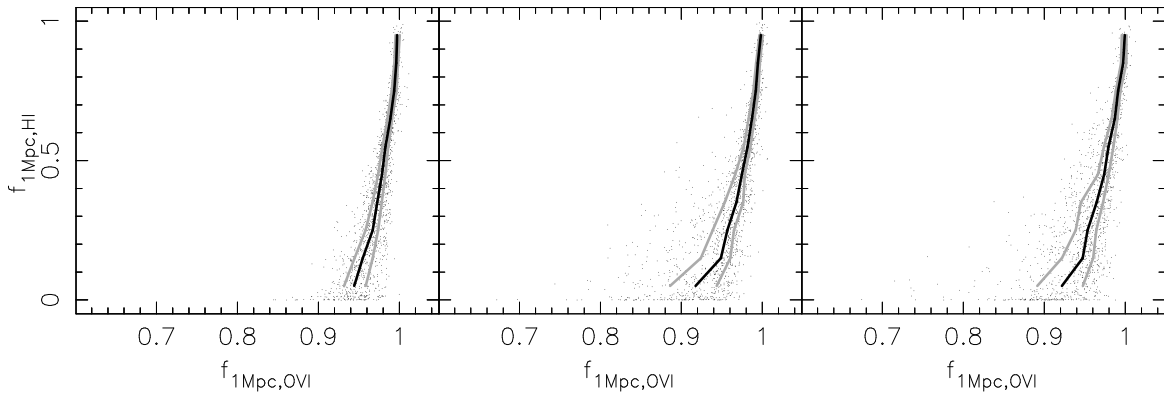


FIG. 16.— The mean transmissivity of the galaxies of HI, $f_{1\text{Mpc,HI}}$ for the pixels within $1 h^{-1}$ comoving Mpc as a function of the mean transmissivity of OVI, $f_{1\text{Mpc,OVI}}$, for models NF (left), SF (middle), and ESF (right). The lines indicate median (black line) and 25th and 75th percentile (grey lines).

and void regions is in a similar thermal state.

Figure 6 shows that the extremely strong SN feedback in model ESF develops a much stronger galactic wind and a larger hot gas bubble. Feedback is now strong enough to affect the filaments. Gas accretion through the filaments is suppressed, so that star formation in the central galaxy ceases (Fig. 3). However, even here the denser regions of the filaments survive, and the density distribution of HI is similar to the one seen in models NF and SF. Figure 9 reveals that in model ESF there is more collisionally ionized OVI especially in the region close to the galaxy ($r \leq 40$ kpc) where the OVI weighted temperature is around $\text{Log}(T(\text{K}))=5.5$ and the OVI density peaks.

Figures 11-13 represent the spectra whose LOS are chosen as the 5×5 grid points each separated by 50 proper kpc projected on the sky i.e., in the X-Y plane. In the

figures, the middle panels correspond to the LOS through the center of the galaxy. First, we compare HI absorption lines between the three models. At the LOS through the central galaxy, the HI lines are heavily saturated, i.e., they produce a damped Lyman alpha line, except in model ESF. In model ESF, not enough cold gas can survive in the galaxy due to the extremely strong feedback. In all the models, the HI absorption becomes weaker with the projected distance from the galaxy. General features of HI absorption lines are similar among the three models. Thus, the signature of a galactic wind seems to be difficult to see in HI absorption lines, confirming the conclusions of previous studies (Theuns et al. 2002; Croft et al. 2002; Bruscoli et al. 2003; Kollmeier et al. 2006).

However, a more detailed comparison of HI absorption line features between models NF and SF (Figs. 11 and 12, respectively) shows that the HI absorption lines tend

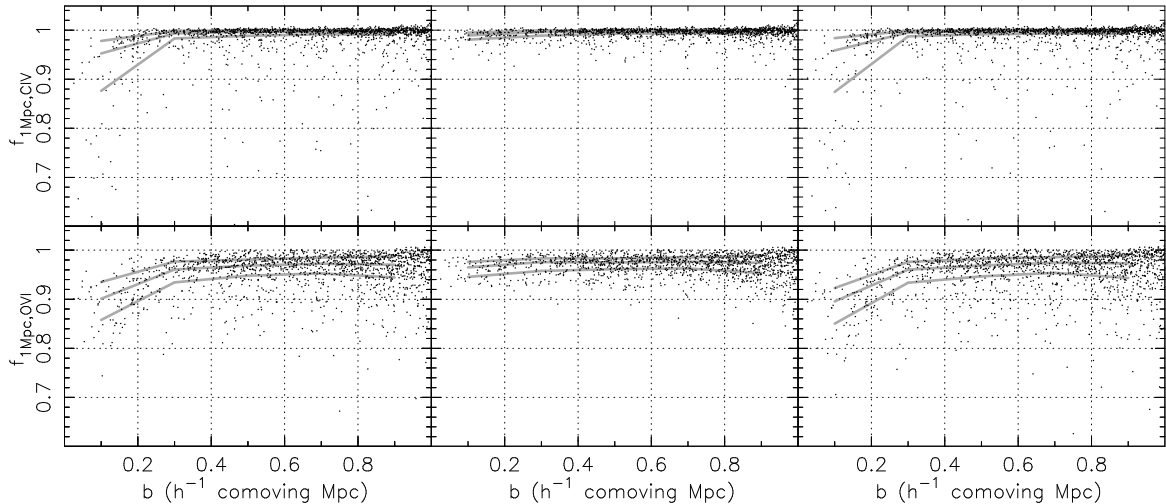


FIG. 17.— The mean transmissivity of CIV (upper), and OVI (lower) for the pixels within $1 h^{-1}$ comoving Mpc of the galaxies as a function of the impact parameter. The left panel shows the result of model SF. The middle panel presents the result of model SF, when the IGM is assumed to be homogeneously enriched at the level of $[C/H]=-2.5$ and $[O/H]=-3$. The right panel demonstrates the result of model SF, when the QSO only UV background radiation suggested by Haardt & Madau (2001) is adopted. The gray lines indicate median and 25th and 75th percentile.

to be stronger in model SF than those in model NF, even close to the galaxy. This is a counter-intuitive result, because it seems natural that a strong wind should predominantly be destroying HI clouds, as suggested by Adelberger et al. (2003) and Bertone & White (2006). However, as shown in Figures 2 and 5, strong feedback redistributes the high density gas in the galaxy to the surrounding region, and the filaments become broader. This leads to the stronger HI lines in model SF, especially in the outer regions of the galaxy. A similar effect is seen in model ESF (Fig.13). Therefore, we suggest that stronger SN feedback actually increases the HI absorption. We will test this more quantitatively in the next section.

Conversely, we do see a lack of neutral hydrogen along some LOS close to the galaxy. However, they do not seem to have anything to do with winds. In model NF, the LOS at $(X, Y) = (-100, -50)$ and $(-100, -100)$ have very weak HI absorption lines, although their projected distance is smaller than ~ 120 proper kpc ($\sim 300 h^{-1}$ comoving kpc). Adelberger et al. (2005a) studied HI absorption lines around star-forming galaxies at $2 \leq z \leq 3$, and found that some LOS which are within $1 h^{-1}$ comoving Mpc from the galaxies show weak or absent HI absorption. They argue that such a lack of absorption may be caused by a galactic superwind destroying the neutral hydrogen. However, our model NF does *not* include any SN feedback. The LOS at $(X, Y) = (-100, -50)$ corresponds to the line at $X = -100$ in the lower panels of Figures 4 and 7. This LOS passes through hot accretion-shocked gas which cannot accommodate HI, and misses the more HI-rich filaments. This example demonstrates that it is possible to have LOS close to galaxies which do not show any strong HI absorption, without the need for a galactic wind.

It is also worth mentioning that there are some LOS which show double HI absorption lines, especially in model NF, e.g., the LOS at $(X, Y) = (50, 0)$. We find that this is due to symmetric gas infall from the filaments. The LOS at $(X, Y) = (50, 0)$ in model NF can be seen at $X = 50$ kpc at the middle panels of Figure 7. This

LOS passes through two filaments at $Z \sim -120$ and ~ 75 kpc, and the velocity map shows the filament at $Z \sim -100$ (~ 75) has positive (negative) LOS velocity. As a result, these two filaments appear as double absorption components. Such double HI absorption line features become less obvious in the cases of stronger feedback, because outflow from the galaxy makes the velocity field more chaotic, and fills the gap between the components in velocity space.

We also compare CIV and OVI lines among the models. In model NF, there are almost no CIV or OVI lines at $R \geq 50$ proper kpc. The LOS at $(X, Y) = (50, -50)$ shows strong CIV lines. However, this is due to the next closest galaxy, as seen in Figure 7. In contrast, the stronger feedback in models SF and ESF creates CIV and OVI lines further away from the galaxy. We also investigated the absorption lines with a much finer grid of LOS, i.e., smaller separations, and found that strong CIV or OVI lines are rare at projected radii $R \geq 100$ kpc even in models SF and ESF, unless there is another galaxy close to the LOS. This can also be seen in Figures 8 and 9, where dense CIV and OVI regions extent to about 100 kpc. OVI lines are very rare in model NF, and only exist where the HI absorption is saturated. On the other hand, strong feedback models produce more OVI lines, that are sometimes stronger than CIV lines. These figures demonstrate that the OVI lines are the most sensitive signature of a galactic wind in absorption. We study this possibility more quantitatively in the next section.

3.2. The mean transmissivity of HI, CIV, and OVI

In this section, we analyze the artificial QSO spectra in 1000 random LOS. Since our simulation volume is a spherical volume (Sec. 2.2), we cannot use the LOS at too large an impact parameter. Therefore, we generate 1000 spectra for the random LOS at the projected radius of $R < 400$ proper kpc. We also change the angle of projection randomly for each LOS.

Within the three dimensional radius of $r = 400$ proper kpc, the high-resolution volume of the simulations contains two galaxies whose virial mass is more than 10^{11}

M_{\odot} . Since the virial mass of the observed UV-selected galaxies is not well known, as mentioned above (see also Erb et al. 2006), we assume these two galaxies are such galaxies, and apply a similar analysis to the one done for the observed UV-selected galaxies (Adelberger et al. 2003, 2005a). Adelberger et al. (2005a) measured the mean transmissivity of all HI pixel in their QSO spectra that lie within $1 h^{-1}$ comoving Mpc from the galaxies as determined from the projected distance and the LOS velocity. In this paper we indicate the mean transmissivity as $f_{1\text{Mpc}}$. We analyze $f_{1\text{Mpc}}$ not only for HI ($f_{1\text{Mpc,HI}}$) but also for CIV ($f_{1\text{Mpc,CIV}}$) and OVI ($f_{1\text{Mpc,OVI}}$) for all the LOS spectra for our two galaxies. In reality, it is difficult to measure $f_{1\text{Mpc}}$ for metal lines. For example, OVI lines are often contaminated by interloper Lyman alpha lines. However, we carry out this theoretical exercise to understand the effect of galactic winds on absorption lines quantitatively.

Figure 14 shows the mean transmissivity of HI, CIV, and OVI as a function of the projected distance from the galaxy, i.e., the impact parameter, b . Figure 15 shows the histogram of the probability of the decrement which is defined as $1 - f_{1\text{Mpc}}$ from Figure 14. The top panels of Figures 14 and 15 correspond to the lower panel of Figures 13 and 15 of Adelberger et al. (2005a), respectively. The left-top panel of Figure 15 shows results similar to those from previous numerical simulation studies with without feedback (Kollmeier et al. 2003; Tasker & Bryan 2006). Although the observational data (dotted histogram) of Adelberger et al. (2005a) agree as far as strong absorption is concerned, their data show a much higher probability for the very weak absorption ($1 - f_{1\text{Mpc}} < 0.2$). Adelberger et al. (2005a) claim that this may be because in the real universe galactic winds turn moderate absorption into weak absorption, but do not affect the strong absorption systems. However, as seen in the top panels of Figures 14 and 15, our simulations predict that the existence of the strong galactic wind does not change the mean flux transmissivity of the HI lines. Interestingly, if we compare the transmissivity at the LOS close to the galaxy ($b \leq 0.4h^{-1}$ comoving Mpc) in Figure 14, the stronger feedback leads to slightly stronger mean absorption, i.e., smaller median $f_{1\text{Mpc,HI}}$, although the difference is subtle. Therefore, again, we conclude that HI absorption lines generally are unaffected by galactic winds. This leaves an inconsistency between the observations and numerical simulations. Unfortunately, the current number of the observational sample is not satisfactory (31 systems in Adelberger et al. 2005a) to reach firm conclusions. On the theory side, the implementation of feedback has been one of the more uncertain ingredients in current numerical simulations (e.g. Okamoto et al. 2005; Kobayashi et al. 2006; Scannapieco et al. 2006a). We adopt the simplest implementation, but different implementations may lead to different conclusions. Clearly, further observational studies and numerical simulations are required to address this problem.

Figures 14 and 15 also show the results for CIV and OVI lines, which appear to be more sensitive to the effect of SN feedback. Model NF shows low $f_{1\text{Mpc,CIV}}$ to be almost independently of the impact parameter. On the other hand, models SF and ESF show that significantly more LOS have a lower $f_{1\text{Mpc,CIV}}$ at $b < \sim 0.2h^{-1}$ comoving Mpc. The mean transmissivity of OVI lines also

shows a similar trend. However, for OVI the absorption becomes noticeably stronger i.e., $f_{1\text{Mpc,OVI}}$ decreases, as the impact parameter decreases below $b < \sim 0.4h^{-1}$ comoving Mpc. Figure 15 reveals that model NF barely shows a decrement $1 - f_{1\text{Mpc}}$ higher than 0.2 for both CIV and OVI, but models SF and ESF can produce such strong absorption lines. However, note that y-axis of the figure is the logarithm of probability, and it represents only $\sim 1\%$ of $f_{1\text{Mpc}}$ that show such strong absorption in models SF and ESF.

In the previous section, we suggested that OVI is a good tracer for a galactic wind, and in model NF OVI lines are only observable where the HI lines are saturated. On the other hand, models SF and ESF produce OVI lines even where the HI is not saturated. Figure 16 plot the $f_{1\text{Mpc,HI}}$ against $f_{1\text{Mpc,OVI}}$. Figure clearly shows that models SF and ESF show the significant fraction of the spectra with relatively weak HI ($f_{1\text{Mpc,HI}} > 0$) and stronger OVI ($f_{1\text{Mpc,OVI}} < 0.95$). We have calculated the probability of low $f_{1\text{Mpc,OVI}}$ for the spectra with $f_{1\text{Mpc,HI}} > 0.2$. Model NF has only 14 % of the spectra with $f_{1\text{Mpc,OVI}} < 0.95$, while models SF and ESF have 24 and 28 %. Although the difference is small, the stronger feedback seems to produce more such HI weak OVI strong lines.

Finally, we briefly mention how our results are sensitive to the distribution of metals and the assumed UV background radiation. Since re-simulations changing the metal yields and the UV background radiation are computationally too expensive, we analyzed the results of model SF, assuming different metal distributions and UV background radiations. Figure 17 shows the results of the same analysis as Figure 14 in the cases when the the IGM is assumed to be homogeneously enriched at the level of $[\text{C}/\text{H}] = -2.5$ and $[\text{O}/\text{H}] = -3$ (model SFhZ) and when the QSO-only UV background radiation suggested by Haardt & Madau (2001) is adopted (model SFQ), while model SF includes radiation from both QSO and galaxies. Model SFhZ demonstrates that if the heavy elements are homogeneously distributed with the assumed metallicity, there is very little correlation between the strength of metal lines and the impact parameter. Therefore, it is important to follow the metal distribution in the IGM self-consistently. Model SFQ shows that $f_{1\text{Mpc,CIV}}$ and $f_{1\text{Mpc,OVI}}$ differ little between the QSO and galaxy radiation and QSO-only UV background radiation cases, except for very subtle decrease in CIV absorptions and increase in OVI absorptions (see also Aguirre et al. 2005).

4. CONCLUSIONS

We have analyzed the QSO absorption features obtained from cosmological numerical simulations with different strengths of SN feedback. Our simulations self-consistently follow the metal exchange histories among the IGM, ISM, and stellar components. We investigate not only the neutral hydrogen absorption lines but also the ionization lines for heavy elements, keeping track of the abundance history of the elements.

We have paid particular attention to the properties of the IGM around high-redshift ($z = 2.43$) galaxies with $M_{\text{vir}} \sim 10^{11} M_{\odot}$. We found that a model without mechanical feedback creates hot gas halos around galaxies due to shock heating, with radii up to 100 proper kpc. We found that such hot gas can lead to a lack of HI

absorption (Fig. 11) even for LOS close to galaxies, as found by Adelberger et al. (2005a), without having to invoke a galactic wind.

In our strong feedback models, outflows induced by SN feedback produce larger hot bubbles around galaxies (Figs. 5 and 6). However, such outflows tends to escape to lower density regions, and hardly affect the dense filaments producing HI absorption systems so that the transmissivity of HI Lyman alpha is virtually independent of the strength of SN feedback. If anything the absorption by neutral hydrogen slightly increases in the presence of a wind. We conclude that the presence or absence of HI absorption lines is not a good indicator of the presence or absence of a galactic wind.

On the other hand, we found that the metal lines, especially OVI, are sensitive to the existence of outflows. Without feedback, it is difficult to enrich the IGM enough to produce strong OVI lines further away from galaxies (Fig. 4), unless there are nearby satellite galaxies intersected by the LOS by chance. We also found that, in the no-feedback model, strong OVI lines are almost always associated with saturated HI lines. On the other hand, the strong feedback model can produce strong OVI lines even where HI lines are unsaturated, because strong feedback can re-distribute the enriched gas to relatively low density regions. We have confirmed this by looking for the spectra whose OVI flux is less than 0.8 over more than 5 pixels and whose mean HI flux within ± 50 km s⁻¹ from the HI velocity corresponding to the OVI lines are higher than 0.2 from 1000 spectra with random LOS.

The no-feedback model has no such spectra, while strong feedback (model SF) has 12 of such spectra. We point out that Figure 9 of Simcoe et al. (2004) shows an OVI line where the HI is not saturated. Our results suggest that this is likely to be a region where the effect of a galactic wind is significant. Analyzing the transmissivity of OVI lines we found that strong feedback creates more LOS with lower transmissivity, i.e. stronger OVI absorption, near the star-forming galaxies. The statistical analysis of transmissivity also shows that there are more LOS where stronger OVI is associated with weaker HI, in the presence of galactic winds. We expect that the pixel-optical depth analysis of OVI against HI (Schaye et al. 2000) would be sensitive to the presence of a galactic wind, and we will test this idea in a future paper. In conclusion, OVI appears a theoretically good tracer of galactic winds that merits further attention.

DK thanks the financial support of the JSPS, through Postdoctoral Fellowship for research abroad. We acknowledge the Center for Computational Astrophysics of the National Astronomical Observatory, Japan (project ID: imm33a), the Institute of Space and Astronautical Science of Japan Aerospace Exploration Agency, and the Australian and Victorian Partnerships for Advanced Computing, where the numerical computations for this paper were performed. MR is grateful to the NSF for support under grant AST-05-06845.

REFERENCES

- Abel, T., Anninos, P., Zhang, Y., & Norman, M. L. 1997, *New Astronomy*, 2, 181
- Adelberger, K. L., Shapley, A. E., Steidel, C. C., Pettini, M., Erb, D. K., & Reddy, N. A. 2005a, *ApJ*, 629, 636
- Adelberger, K. L., Steidel, C. C., Pettini, M., Shapley, A. E., Reddy, N. A., & Erb, D. K. 2005b, *ApJ*, 619, 697
- Adelberger, K. L., Steidel, C. C., Shapley, A. E., & Pettini, M. 2003, *ApJ*, 584, 45
- Aguirre, A., Hernquist, L., Schaye, J., Weinberg, D. H., Katz, N., & Gardner, J. 2001, *ApJ*, 560, 599
- Aguirre, A., Schaye, J., Hernquist, L., Kay, S., Springel, V., & Theuns, T. 2005, *ApJ*, 620, L13
- Aguirre, A., Schaye, J., Kim, T.-S., Theuns, T., Rauch, M., & Sargent, W. L. W. 2004, *ApJ*, 602, 38
- Aguirre, A., Schaye, J., & Theuns, T. 2002, *ApJ*, 576, 1
- Anninos, P., Zhang, Y., Abel, T., & Norman, M. L. 1997, *New Astronomy*, 2, 209
- Arimoto, N., & Yoshii, Y. 1987, *A&A*, 173, 23
- Becker, R. H., Fan, X., White, R. L., Strauss, M. A., Narayanan, V. K., Lupton, R. H., Gunn, J. E., Annis, J., Bahcall, N. A., Brinkmann, J., Connolly, A. J., Csabai, I., Czarapata, P. C., Doi, M., Heckman, T. M., Hennessy, G. S., Ivezić, Z., Knapp, G. R., Lamb, D. Q., McKay, T. A., Munn, J. A., Nash, T., Nichol, R., Pier, J. R., Richards, G. T., Schneider, D. P., Stoughton, C., Szalay, A. S., Thakar, A. R., & York, D. G. 2001, *AJ*, 122, 2850
- Bertone, S., & White, S. D. M. 2006, *MNRAS*, 367, 247
- Bertschinger, E. 2001, *ApJS*, 137, 1
- Brook, C. B., Kawata, D., Gibson, B. K., & Flynn, C. 2004, *MNRAS*, 349, 52
- Bruscoli, M., Ferrara, A., Marri, S., Schneider, R., Maselli, A., Rollinde, E., & Aracil, B. 2003, *MNRAS*, 343, L41
- Cen, R., Kang, H., Ostriker, J. P., & Ryu, D. 1995, *ApJ*, 451, 436
- Cen, R., Nagamine, K., & Ostriker, J. P. 2005, *ApJ*, 635, 86
- Cowie, L. L., & Songaila, A. 1998, *Nature*, 394, 44
- Croft, R. A. C., Hernquist, L., Springel, V., Westover, M., & White, M. 2002, *ApJ*, 580, 634
- Davé, R., Hellsten, U., Hernquist, L., Katz, N., & Weinberg, D. H. 1998, *ApJ*, 509, 661
- Dekel, A., & Birnboim, Y. 2006, *MNRAS*, 368, 2
- Dekel, A., & Silk, J. 1986, *ApJ*, 303, 39
- Erb, D. K., Steidel, C. C., Shapley, A. E., Pettini, M., Reddy, N. A., & Adelberger, K. L. 2006, *ApJ*, 646, 107
- Fan, X., Narayanan, V. K., Lupton, R. H., Strauss, M. A., Knapp, G. R., Becker, R. H., White, R. L., Pentericci, L., Leggett, S. K., Haiman, Z., Gunn, J. E., Ivezić, Z., Schneider, D. P., Anderson, S. F., Brinkmann, J., Bahcall, N. A., Connolly, A. J., Csabai, I., Doi, M., Fukugita, M., Geballe, T., Grebel, E. K., Harbeck, D., Hennessy, G., Lamb, D. Q., Miknaitis, G., Munn, J. A., Nichol, R., Okamura, S., Pier, J. R., Prada, F., Richards, G. T., Szalay, A., & York, D. G. 2001, *AJ*, 122, 2833
- Ferland, G. J., Korista, K. T., Verner, D. A., Ferguson, J. W., Kingdon, J. B., & Verner, E. M. 1998, *PASP*, 110, 761
- Galli, D., & Palla, F. 1998, *A&A*, 335, 403
- Gibson, B. K. 1997, *MNRAS*, 290, 471
- Governato, F., Willman, B., Mayer, L., Brooks, A., Stinson, G., Valenzuela, O., Wadsley, J., & Quinn, T. 2006, *ArXiv Astrophysics e-prints*
- Haardt, F., & Madau, P. 2001, in *Clusters of Galaxies and the High Redshift Universe Observed in X-rays*, ed. D. M. Neumann & J. T. V. Tran
- Ikeuchi, S. 1977, *Progress of Theoretical Physics*, 58, 1742
- Ikeuchi, S., & Ostriker, J. P. 1986, *ApJ*, 301, 522
- Iwamoto, K., Brachwitz, F., Nomoto, K., Kishimoto, N., Umeda, H., Hix, W. R., & Thielemann, F. 1999, *ApJS*, 125, 439
- Johnson, H. E., & Axford, W. I. 1971, *ApJ*, 165, 381
- Kawata, D., Arimoto, N., Cen, R., & Gibson, B. K. 2006, *ApJ*, 641, 785
- Kawata, D., & Gibson, B. K. 2003, *MNRAS*, 340, 908
- Kereš, D., Katz, N., Weinberg, D. H., & Davé, R. 2005, *MNRAS*, 363, 2
- Kitayama, T., & Suto, Y. 1996, *ApJ*, 469, 480
- Kobayashi, C., Springel, V., & White, S. D. M. 2006, *ArXiv Astrophysics e-prints*
- Kobayashi, C., Tsujimoto, T., & Nomoto, K. 2000, *ApJ*, 539, 26
- Kodama, T., & Arimoto, N. 1997, *A&A*, 320, 41
- Kollmeier, J. A., Miralda-Escudé, J., Cen, R., & Ostriker, J. P. 2006, *ApJ*, 638, 52

- Kollmeier, J. A., Weinberg, D. H., Davé, R., & Katz, N. 2003, *ApJ*, 594, 75
- Kriek, M., van Dokkum, P., Franx, M., Quadri, R., Gawiser, E., Herrera, D., Illingworth, G., Labbe, I., Lira, P., Marchesini, D., Rix, H.-W., Rudnick, G., Taylor, E., Toft, S., Urry, M., & Wuyts, S. 2006, *ArXiv Astrophysics e-prints*
- Labbé, I., Huang, J., Franx, M., Rudnick, G., Barmby, P., Daddi, E., van Dokkum, P. G., Fazio, G. G., Schreiber, N. M. F., Moorwood, A. F. M., Rix, H.-W., Röttgering, H., Trujillo, I., & van der Werf, P. 2005, *ApJ*, 624, L81
- Larson, R. B. 1974, *MNRAS*, 169, 229
- Lynds, C. R., & Sandage, A. R. 1963, *ApJ*, 137, 1005
- Madau, P., Ferguson, H. C., Dickinson, M. E., Giavalisco, M., Steidel, C. C., & Fruchter, A. 1996, *MNRAS*, 283, 1388
- Madau, P., Ferrara, A., & Rees, M. J. 2001, *ApJ*, 555, 92
- Martin, C. L. 1998, *ApJ*, 506, 222
- , 2005, *ApJ*, 621, 227
- Mathews, W. G., & Baker, J. C. 1971, *ApJ*, 170, 241
- Ohyama, Y., Taniguchi, Y., Iye, M., Yoshida, M., Sekiguchi, K., Takata, T., Saito, Y., Kawabata, K. S., Kashikawa, N., Aoki, K., Sasaki, T., Kosugi, G., Okita, K., Shimizu, Y., Inata, M., Ebizuka, N., Ozawa, T., Yadoumaru, Y., Taguchi, H., & Asai, R. 2002, *PASJ*, 54, 891
- Ohyama, Y., Taniguchi, Y., Kawabata, K. S., Shioya, Y., Murayama, T., Nagao, T., Takata, T., Iye, M., & Yoshida, M. 2003, *ApJ*, 591, L9
- Okamoto, T., Eke, V. R., Frenk, C. S., & Jenkins, A. 2005, *MNRAS*, 363, 1299
- Oppenheimer, B. D., & Davé, R. 2006, *MNRAS*, 373, 1265
- Pettini, M., Kellogg, M., Steidel, C. C., Dickinson, M., Adelberger, K. L., & Giavalisco, M. 1998, *ApJ*, 508, 539
- Pieri, M. M., Schaye, J., & Aguirre, A. 2006, *ApJ*, 638, 45
- Porciani, C., & Madau, P. 2005, *ApJ*, 625, L43
- Rauch, M., Haehnelt, M. G., & Steinmetz, M. 1997, *ApJ*, 481, 601
- Rauch, M., Sargent, W. L. W., & Barlow, T. A. 2001a, *ApJ*, 554, 823
- Rauch, M., Sargent, W. L. W., Barlow, T. A., & Carswell, R. F. 2001b, *ApJ*, 562, 76
- Raymond, J. C., & Smith, B. W. 1977, *ApJS*, 35, 419
- Robertson, B., Yoshida, N., Springel, V., & Hernquist, L. 2004, *ApJ*, 606, 32
- Rupke, D. S., Veilleux, S., & Sanders, D. B. 2005, *ApJS*, 160, 115
- Scannapieco, C., Tissera, P. B., White, S. D. M., & Springel, V. 2006a, *MNRAS*, 371, 1125
- Scannapieco, E. 2005, *ApJ*, 624, L1
- Scannapieco, E., Ferrara, A., & Madau, P. 2002, *ApJ*, 574, 590
- Scannapieco, E., Pichon, C., Aracil, B., Petitjean, P., Thacker, R. J., Pogosyan, D., Bergeron, J., & Couchman, H. M. P. 2006b, *MNRAS*, 365, 615
- Schaye, J. 2004, *ApJ*, 609, 667
- Schaye, J., Aguirre, A., Kim, T.-S., Theuns, T., Rauch, M., & Sargent, W. L. W. 2003, *ApJ*, 596, 768
- Schaye, J., Rauch, M., Sargent, W. L. W., & Kim, T.-S. 2000, *ApJ*, 541, L1
- Seager, S., Sasselov, D. D., & Scott, D. 1999, *ApJ*, 523, L1
- , 2000, *ApJS*, 128, 407
- Shapley, A. E., Steidel, C. C., Pettini, M., & Adelberger, K. L. 2003, *ApJ*, 588, 65
- Simcoe, R. A., Sargent, W. L. W., & Rauch, M. 2002, *ApJ*, 578, 737
- , 2004, *ApJ*, 606, 92
- Simcoe, R. A., Sargent, W. L. W., Rauch, M., & Becker, G. 2006, *ApJ*, 637, 648
- Sommer-Larsen, J., Götz, M., & Portinari, L. 2003, *ApJ*, 596, 47
- Spiegel, D. N., Bean, R., Dore, O., Nolte, M. R., Bennett, C. L., Hinshaw, G., Jarosik, N., Komatsu, E., Page, L., Peiris, H. V., Verde, L., Barnes, C., Halpern, M., Hill, R. S., Kogut, A., Limon, M., Meyer, S. S., Odegard, N., Tucker, G. S., Weiland, J. L., Wollack, E., & Wright, E. L. 2006, *ArXiv Astrophysics e-prints*
- Tasker, E. J., & Bryan, G. L. 2006, *ApJ*, 642, L5
- Theuns, T., Viel, M., Kay, S., Schaye, J., Carswell, R. F., & Tzanavaris, P. 2002, *ApJ*, 578, L5
- van den Hoek, L. B., & Groenewegen, M. A. T. 1997, *A&AS*, 123, 305
- Veilleux, S., Cecil, G., & Bland-Hawthorn, J. 2005, *ARA&A*, 43, 769
- Veilleux, S., Shopbell, P. L., Rupke, D. S., Bland-Hawthorn, J., & Cecil, G. 2003, *AJ*, 126, 2185
- Woolsey, S. E., & Weaver, T. A. 1995, *ApJS*, 101, 181